THE ASTROPHYSICAL JOURNAL, 489:744–752, 1997 November 10

A RADIO JET–H_2O MASER SYSTEM IN W75N(B) AT A 200 AU SCALE: EXPLORING THE EVOLUTIONARY STAGES OF YOUNG STELLAR OBJECTS

JOSÉ M. TORRELLES
Instituto de Astrofisica de Andalucía, CSIC, Apdo. Correos 3004, E-18080 Granada, Spain; torrelles@iaa.es
JOSÉ F. GÓMEZ
Laboratorio de Astrofisica Espacial y Física Fundamental, INTA, Apdo. Correos 50727, E-28080 Madrid, Spain; jfg@laeff.esa.es
LUIS F. RODRÍGUEZ
Instituto de Astronomía, UNAM, Apdo. Postal 70-264, DF 04510, México; luisfr@astrosmo.unam.mx
PAUL T. P. HO
Harvard-Smithsonian Center for Astrophysics, 60 Garden Street, Cambridge, MA 02138; ho@cfaho1.harvard.edu
SALVADOR CURIEL
Instituto de Astronomía, UNAM, Apdo. Postal 70-264, DF 04510, México; scuriel@astroscu.unam.mx
AND
ROBERTO VÁZQUEZ
Instituto de Astrofisica de Andalucía, CSIC, Apdo. Correos 3004, E-18080 Granada, Spain; vázquez@iaa.es
Received 1997 April 28; accepted 1997 June 24

ABSTRACT

We have observed simultaneously with the VLA in its A configuration the 1.3 cm continuum and H_2O maser emission toward the star-forming region W75N(B) with 0.″1 resolution using a powerful cross-calibration technique. Three continuum sources (VLA 1, VLA 2, and VLA 3) were detected in a region of 1.″5. VLA 1 is elongated (0.″43 × 0.″12) approximately in the direction of the bipolar molecular outflow observed at scales of 2′. The frequency dependence of the flux density and size are consistent with an optically partially thick ionized thermal biconical jet. VLA 2 appears unresolved, while VLA 3 shows a bright core plus extended emission. We detected 29 H_2O maser spots (spatial components) in a region of 13″ × 7″ around W75N(B). These masers are mainly distributed in two clusters, one associated with VLA 1 (11 maser spots), and the other one associated with VLA 2 (eight maser spots). One H_2O maser spot is associated with VLA 3. The masers associated with VLA 1 are distributed along the major axis of the radio jet. We conclude that VLA 1 is the powering source of the extended bipolar molecular outflow and that the water masers along the radio jet axis are delineating the outflow at scales of 1″. On the other hand, the eight masers coincident with VLA 2 are distributed in a shell of 0.″18 × 0.″10, with a rough north-south velocity segregation that could indicate bound motions around this continuum source. From the comparison of H_2O and OH maser distribution in the region with respect to the three radio sources, we consider an evolutionary scheme in which H_2O masers are excited in gravitationally bound material (e.g., in circumstellar disks) in less evolved young stellar objects (YSOs), while in more evolved YSOs H_2O masers preferentially trace outflows.

Subject headings: H II regions — ISM: individual (W75N) — ISM: jets and outflows — masers — stars: formation

1. INTRODUCTION

Young stellar objects (YSOs) and protostars are embedded in large amounts of circumstellar matter, often rendering them invisible at optical, and sometimes even at near-infrared, wavelengths. However, most of the embedded YSOs can be detected with the Very Large Array (VLA) at centimeter wavelengths, with flux densities at the millijansky level (e.g., Pravdo et al. 1985; Rodríguez et al. 1990; Gómez et al. 1994; and for reviews Anglada 1995, 1996). This radio continuum emission could be due to circumstellar gas that has been shock ionized by a stellar wind associated with the earliest stages of star formation (Torrelles et al. 1985; Curiel et al. 1989). Indeed, in a few cases, when observed with angular resolutions $\lesssim$0.″5, these radio sources appear to be elongated at scales of $\lesssim$1000 AU, in the direction parallel to the large-scale ($\sim$0.1–1 pc) molecular outflows. If these are radio jets, their collimation could be the result of magnetohydrodynamic processes within an accretion disk (e.g., Lizano & Torrelles 1995 and references therein). Furthermore, these jets could drive the large-scale outflows commonly observed in star-forming regions (see Chernin & Masson 1991; Raga et al. 1993). However, the faintness of these jets allowed only a few cases to be studied with the VLA with regard to their spatial and spectral characteristics. For HH 1-2 VLA 1, Cepheus A HW2, Serpens, and HH 80-81, the frequency dependence of the flux density and the size of the jets, $S_\nu \propto \nu^\alpha$ ($\alpha \simeq 0.3$–0.7) and $\theta \propto \nu^{-\beta}$ ($\beta \simeq 0.6$–1), have been determined to be consistent with models of thermal radio jets (Rodríguez et al. 1990, 1994; Curiel et al. 1993; Martí, Rodríguez, & Reipurth 1993, 1995; Torrelles et al. 1996; see Anglada 1996 for a review and Reynolds 1986 for thermal bipolar jet models).

The combination of faintness and small size scale of the radio jets (e.g., 100 AU at a distance of 500 pc is 0.″2) requires essentially high-frequency observations with high sensitivity to provide the needed angular resolution to study this emission. An angular resolution better than $\sim$0.″1 can be achieved with the VLA in its A configuration at

7 mm and 1.3 cm. The present sensitivity of the VLA 7 mm system, with only 13 antennas, is not good enough for a detailed study of these weak objects. However, this study is possible at 1.3 cm if calibration is perfect. Fortunately, the atmospheric seeing effects at this frequency can be fully compensated for when a strong H_2O maser ($\lambda = 1.3$ cm) is present within the primary beam. Observing simultaneously the continuum emission and the H_2O maser, the latter can be used as the amplitude and phase reference. This powerful cross-calibration technique, introduced by Reid & Menten (1990) to study evolved stars, has been applied successfully to study with 0.″08 resolution both the Cepheus A HW2 thermal radio jet and the relative positions between the H_2O masers and the jet with an accuracy of ~ 1 mas (Torrelles et al. 1996).

Pursuing this cross-calibration technique, we have now observed with the VLA in its A configuration the 1.3 cm continuum and H_2O maser emission toward W75N, having in mind the following general goals: (1) to image the continuum emission of the YSOs with $\sim 0.''1$ resolution; (2) to find new radio jets in YSOs, measuring their degree of collimation; (3) to make a statistical study of the presence of radio jets in YSOs, testing the hypothesis that thermal radio jets are *always* present in outflow regions; and (4) to study the spatio-kinematic distribution of the H_2O masers around YSOs, and their relation to the radio continuum emission. Both circumstellar disks (Torrelles et al. 1996; Fiebig et al. 1996) and high-velocity outflows at 10^2–10^4 AU scales (Gwinn 1994; Chernin 1995) have been inferred previously from the distribution of the H_2O masers. What possible causes could produce this dichotomy in the relation between H_2O masers and thermal jets?

In this paper we report the results obtained toward W75N, located at 2 kpc distance in the Cygnus X complex. This active high-mass star formation region shows strong infrared emission (Wynn-Williams, Becklin, & Neugebauer 1974; Harvey, Campbell, & Hoffmann 1977), an integrated IRAS luminosity of a few times $10^5\ L_\odot$ (Moore et al. 1988), a number of radio continuum sources (Habing et al. 1974; Haschick et al. 1981; Hunter et al. 1994), H_2O masers (Johnston, Sloanaker, & Bologna 1973; Hunter et al. 1994; Lekht 1995; Tofani et al. 1995), OH masers (Haschick et al. 1981; Baart et al. 1986), as well as a CS core and a CO bipolar outflow (Hunter et al. 1994). Of the three 6 cm continuum sources, namely, W75N(A), W75N(B), and W75N(C), only W75N(B) appears to be associated with OH and H_2O masers (Haschick et al. 1981) and a bright 2 μm source (Moore et al. 1988). Haschick et al. (1981) suggested that W75N(B) is excited by a binary protostellar system and that the OH masers are tracing a rotating disk of $\simeq 2''$ size ($\simeq 4000$ AU) surrounding the binary system. Hunter et al. (1994) show that W75N(B) is mainly composed of two sources, W75N(Ba) and W75N(Bb), almost unresolved at 3.6 cm with 0.″5 resolution while separated by $\sim 1.''5$. These could be ultracompact (UC) H II regions, excited by B1 stars. These authors also mapped five H_2O maser components around W75N(B), favoring the model of a shocked disk surrounding the two UC H II regions. The presence of an expanding and rotating disk has also been suggested by Lekht (1995) from H_2O maser variability studies. However, Baart et al. (1986), through MERLIN OH maser observations, favor a scenario in which the OH and H_2O masers are tracing an outflow rather than a rotating disk surrounding W75N(B).

With the 1.3 cm continuum and H_2O maser data presented in this paper, we address three specific questions regarding W75N(B): (1) Which is the powering source of the bipolar molecular outflow observed in the region? (2) What is the origin of the radio continuum emission (e.g., UC H II regions versus ionized stellar winds)? (3) What is the relationship between H_2O and OH masers? In § 2 we present the observations, calibration, and reduction procedure. The results of both the 1.3 cm continuum and H_2O maser data are presented in § 3. Their implications are discussed in § 4. In § 5 we compare the H_2O and OH maser distributions. A possible evolutionary scenario explaining the H_2O maser distribution with respect to the radio sources is presented in § 6. The main conclusions of our study are presented in § 7.

2. OBSERVATIONS

The observations were made with the VLA of the National Radio Astronomy Observatory (NRAO)[1] in the A configuration on 1996 December 15, during a run of 7 hr. We used the four intermediate frequency (IF) spectral line mode of the VLA. Both the right and left circular polarizations were sampled with a bandwidth of 25 MHz, providing seven channels of 3.125 MHz each, and as well as with a bandwidth of 3.125 MHz, with 63 channels of 48.8 kHz each. The broad bandwidth was centered at the frequency 22285.080 MHz for continuum measurements, while the "narrow" bandwidth was centered at the frequency of the H_2O $6_{16} \rightarrow 5_{23}$ maser line (22235.080 MHz) with $V_{LSR} = 10$ km s^{-1}, the ambient cloud velocity. The phase center of the observations was $\alpha(1950) = 20^h36^m50^s.045$, $\delta(1950) = 42°26'57''.873$, which corresponds to a position almost in between the two 3.6 cm continuum maxima of W75N(B) observed by Hunter et al. (1994). The flux and phase calibrators were 3C 48 (adopted flux density = 1.2 Jy at 1.3 cm) and 2021+317 (observed flux density = 2.5 Jy), respectively.

Using the Astronomical Image Processing System (AIPS), initial calibration was done separately for each pair of IFs to remove electronic phase differences between IFs and obtain spectral bandpass corrections. Once the strongest H_2O maser component was identified in a particular spectral channel of the narrow bandwidth, we self-calibrated its signal in phase and amplitude. The phase and amplitude corrections as a function of time, at 10 s intervals, were then applied to both the narrow and broad bandwidth, removing both atmospheric and instrumental errors. With this technique we achieved a dynamic range of $\sim 13{,}000$ for the velocity channel map where the strongest H_2O maser component appears (226 Jy at $V_{LSR} = 13.3$ km s^{-1} with 0.66 km s^{-1} velocity resolution, rms = 17 mJy).

Three continuum sources were detected with the broad bandwidth data. The achieved rms noise was 0.16 mJy, similar to the expected theoretical thermal noise, ~ 0.13 mJy. We note that with cross-calibration, we improved the S/N ratio of the continuum data by a factor of 1.6. In addition, the structure of the radio sources were cleaner and sharper in appearance, demonstrating the improvement in radio seeing.

All maps shown here for both the continuum (§ 3.1) and H_2O masers (§ 3.2) have been cross-calibrated and cleaned

[1] The NRAO is operated by Associated Universities Inc., under cooperative agreement with the National Science Foundation.

using AIPS standard procedures. In particular, individual spectral channel maps were made from the 3.1 MHz bandwidth. The resulting cube (63 channels) of the H_2O maser line was then Hanning smoothed, giving a final velocity resolution of $\simeq 1.2$ km s^{-1}. This smoothing in velocity was applied to reduce the Gibbs ringing effect due to the strong and narrow H_2O masers (see Thompson, Moran, & Swenson 1986 for a discussion of these effects). These Hanning-smoothed data were used to analyze the spatio-kinematic distribution of the H_2O masers in the region.

3. RESULTS

3.1. 1.3 cm *Continuum Emission*

In Figure 1 we show a contour map of the continuum emission with natural weighting of the 25 MHz bandwidth (u, v) data (the "effective" bandwidth was 21.9 MHz, 7 channels × 3.125 MHz). The synthesized beam is 0.″1, and the achieved rms noise of the image is 0.16 mJy beam^{-1}. Three sources are detected. We will call them hereafter, from north to south, VLA 1, VLA 2, and VLA 3, respectively. VLA 1 is elongated, with a deconvolved size of $\sim$0.″4 × 0.″1 (P.A. 43°), while VLA 3 shows a bright core plus extended emission, with a deconvolved size of 0.″09 × 0.″04 (P.A. 152°). VLA 2 appears unresolved ($\lesssim$0.″1). In Table 1 the observed and derived parameters of these three sources at 1.3 cm are listed.

The positions of VLA 1 and VLA 3, coincide, respectively, with the sources W75N(Ba) and W75N(Bb) detected previously at 3.6 cm with 0.″5 resolution by Hunter et al. (1994) and indicated by crosses in Figure 1. On the other hand, VLA 2 lies almost in between VLA 1 and VLA 3 but was not detected previously at 3.6 cm. By convolving our 1.3 cm data with an elliptical Gaussian to give an angular resolution similar to that of the 3.6 cm data (0.″5; Hunter et al. 1994), the resulting map (Fig. 2) resembles that presented at 3.6 cm (although no emission is evident at the position of VLA 2 in the 3.6 cm map). Note that the elongation of VLA 1 in the northeast-southwest direction remains evident at 0.″5 angular resolution. The feature at 3 σ level ($\sim$2 mJy), $\sim$1.″5 south of VLA 3 (Fig. 2), coincides with the source W75N(Bc), a continuum source with 0.85 mJy at 3.6 cm (Hunter et al. 1994). This feature was not significant in our unconvolved 1.3 cm continuum map.

By comparing flux densities obtained at 3.6 and 1.3 cm, we obtain spectral indices $\alpha_{(3.6-1.3\,\mathrm{cm})} = 0.7 \pm 0.1$, $\gtrsim 1$, and $= 1.5 \pm 0.1$ ($S_\nu \propto \nu^\alpha$), for VLA 1, VLA 2, and VLA 3, respectively (Table 1). To estimate the spectral index for VLA 2 we have adopted from the 3.6 cm data (Hunter et al. 1994) an upper 3 σ level of 0.6 mJy at this wavelength. The physical implications from the 1.3 cm continuum detections, as well as from the parameters derived for these three radio sources, will be discussed in § 4.

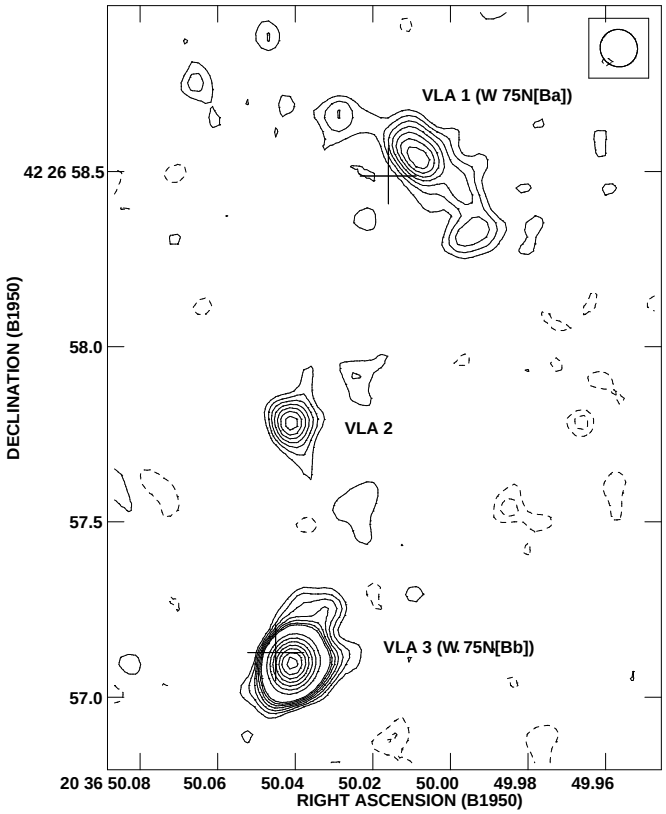

FIG. 1.—1.3 cm continuum contour map of W75N(B). Contours are −3, −2, 2, 3, 4, 5, 6, 7, 8, 15, 20, 25, 30, 35, 40, 45 times 0.16 mJy beam^{-1}, the rms of the map (beam = 0.″1, shown in the top right-hand corner). Three continuum sources are detected, namely, from north to south, VLA 1, VLA 2, and VLA 3, respectively. Crosses indicate the position of the two 3.6 cm continuum sources detected by Hunter et al. (1994) in the area, namely, W75N(Ba) and W75N(Bb), respectively.

3.2. H_2O *Masers*

With a synthesized beam of $\simeq$0.″08 (uniform weighting of the [u, v] data), we have detected 29 H_2O maser spots (spatial components) in a region of $\simeq$13″ × 7″ (0.13 × 0.07 pc, R.A. × decl.) around W75N(B). Most of these maser spots have a single velocity component. H_2O maser emission is observed in the velocity range $V_{LSR} = -5.8$–25.1 km s^{-1}, with the strongest component with intensity $S_\nu = 148.9$

TABLE 1

RADIO CONTINUUM SOURCES AT $\lambda = 1.3$ cm IN W75N(B)

SOURCE	POSITION[a] α(1950)	POSITION[a] δ(1950)	PEAK (1.3 cm) (mJy beam^{-1})	S_ν (1.3 cm)[b] (mJy)	DECONVOLVED SIZE[c] ($\lambda = 1.3$ cm) (arcsec)	S_ν (3.6 cm)[b] (mJy)	SPECTRAL INDEX
VLA 1.....	20 36 50.0056	42 26 58.507	1.42	7.8 ± 0.5	0.43 × 0.12 (43°)	4.0 ± 0.25	0.7 ± 0.1
VLA 2.....	20 36 50.0405	42 26 57.783	1.40	1.6 ± 0.2	≤0.1	≤0.6	≥1.0[d]
VLA 3.....	20 36 50.0406	42 26 57.095	7.59	11.9 ± 0.4	0.09 × 0.04 (152°)	2.7 ± 0.25	1.5 ± 0.1

[a] Position of the 1.3 cm continuum peak. Units of right ascension are hours, minutes, and seconds, and units of declination are degrees, arcminutes, and arcseconds. Relative position errors depend on the signal-to-noise ratio of the emission but are typically $\simeq$3 mas.

[b] Total flux density. The values at 3.6 cm are from Hunter et al. 1994.

[c] The numbers in parentheses are the position angles.

[d] We have adopted a 3 σ upper limit of 0.6 mJy at 3.6 cm (Hunter et al. 1994).

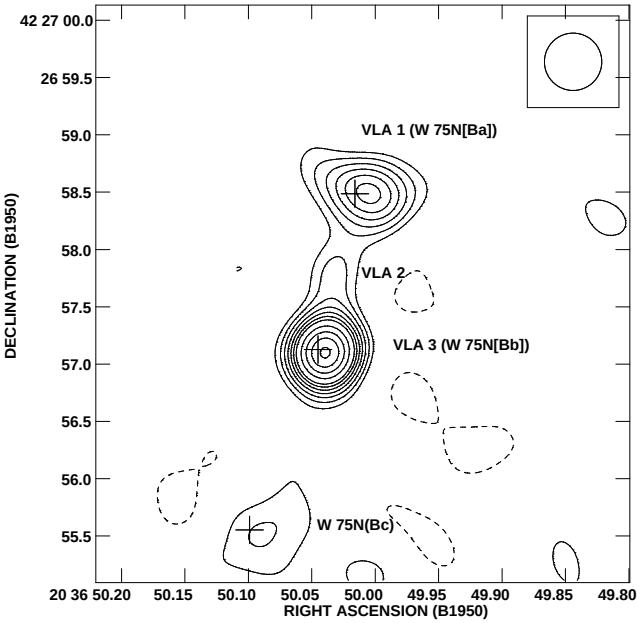

FIG. 2.—1.3 cm continuum contour map with 0.″5 resolution. Crosses indicate the position of the three 3.6 cm continuum sources detected by Hunter et al. (1994) in the area, namely, W75N(Ba), W75N(Bb), and W75N(Bc), respectively.

Jy and $V_{LSR} = 13.3$ km s^{-1}. Intensity, peak position (which was obtained using the task IMFIT of AIPS), and velocity channel of the peak intensity of these H_2O maser spots are listed in Table 2. Line widths of the H_2O masers are ≤ 1.2 km s^{-1}.

Most of these H_2O maser spots are new detections, unseen previously [e.g., Hunter et al. 1994 detected only five distinct spatial components in a field of $\sim 15''$ around W75N(B)]. This is certainly due to the high angular resolution and the high dynamic range of the data presented in this paper (the rms of the channel maps ranges from ~ 12 mJy beam^{-1} for the channel where the strongest maser spot appears, to ~ 5 mJy beam^{-1} for the channels with the weakest H_2O maser components).

TABLE 2

H_2O MASERS IN W75N(B)

POSITION[a]		V_{LSR}	FLUX DENSITY
α(1950)	δ(1950)	(km s^{-1})	(Jy)
20 36 49.5481.....	42 26 55.153	−5.8	0.7
20 36 49.5481.....	42 26 55.153	−1.9	0.3
20 36 49.5499.....	42 26 55.213	+25.1	1.3
20 36 49.5535.....	42 26 59.993	+10.0	10.5
20 36 49.5571.....	42 26 54.933	+3.4	0.09
20 36 49.9781.....	42 26 58.113	+12.6	4.3
20 36 49.9781.....	42 26 58.173	+10.7	9.9
20 36 49.9890.....	42 26 58.453	+15.9	0.7
20 36 49.9908.....	42 26 58.273	+11.3	0.1
20 36 49.9926.....	42 26 58.333	+10.0	1.1
20 36 49.9944.....	42 26 58.493	+13.3	127.4
20 36 50.0016.....	42 26 58.353	+13.3	0.3
20 36 50.0034.....	42 26 58.553	+13.3	148.9
20 36 50.0071.....	42 26 58.773	+9.3	2.7
20 36 50.0360.....	42 26 56.973	+10.7	0.06
20 36 50.0360.....	42 26 57.873	+4.1	0.07
20 36 50.0396.....	42 26 57.773	+14.0	3.1
20 36 50.0414.....	42 26 57.713	+14.6	1.0
20 36 50.0414.....	42 26 57.873	+11.3	1.8
20 36 50.0450.....	42 26 57.893	+7.4	49.0
20 36 50.0468.....	42 26 57.753	+10.7	0.5
20 36 50.0468.....	42 26 57.793	+4.7	0.2
20 36 50.0468.....	42 26 57.853	+1.4	5.0
20 36 50.0468.....	42 26 57.853	−4.5	1.1
20 36 50.0504.....	42 26 59.113	+21.9	0.2
20 36 50.0540.....	42 26 59.113	+10.0	11.2
20 36 50.0811.....	42 27 00.833	+10.7	0.1
20 36 50.0848.....	42 27 00.773	+9.3	0.3
20 36 50.0992.....	42 27 01.613	+10.7	0.5
20 36 50.1010.....	42 27 01.633	+14.0	4.3
20 36 50.6847.....	42 27 01.173	+2.8	0.03

[a] Units of right ascension are hours, minutes, and seconds, and units of declination are degrees, arcminutes, and arcseconds. Relative position errors depend on the signal-to-noise ratio of the emission but are typically $\simeq 1$ mas.

A map showing the positions of the 29 H_2O masers (*crosses*) and the 1.3 cm continuum sources (*squares*) is given in Figure 3. From this figure we see that the H_2O masers are

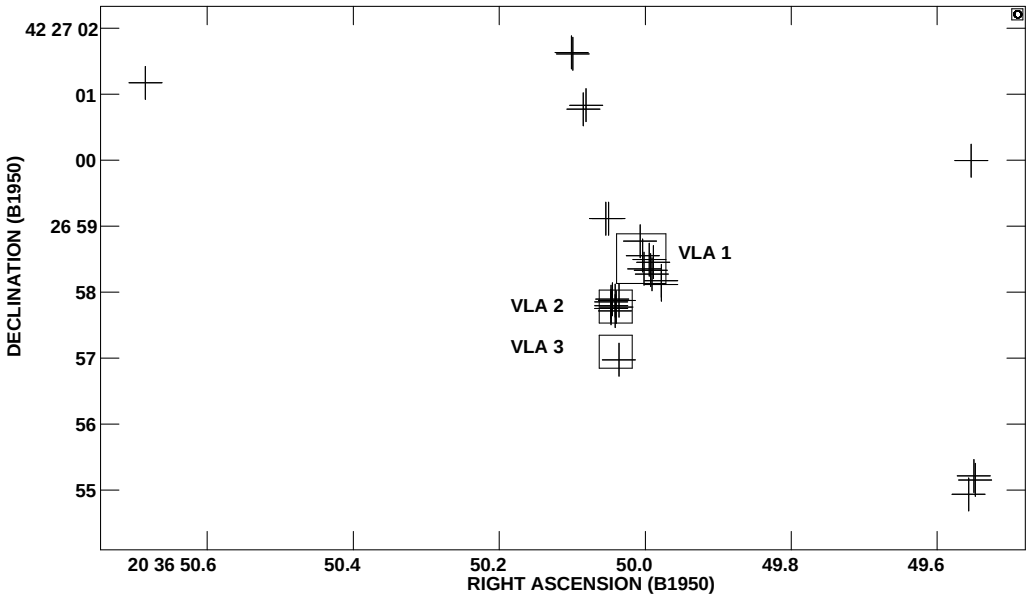

FIG. 3.—Map showing the position of the H_2O masers detected in the region (*crosses*) and the 1.3 cm continuum sources (*squares*; VLA 1, VLA 2, and VLA 3, from north to south).

mainly distributed in two clusters. One cluster is spatially coincident with VLA 1 (11 H_2O maser spots), including the two strongest maser spots of the region, $S_\nu = 148.9$ Jy and 127.4 Jy, both with $V_{LSR} = 13.3$ km s^{-1} (Table 2). The other cluster is spatially coincident with VLA 2 (eight H_2O maser spots), which includes the third strongest maser of the region, $S_\nu = 49.0$ Jy with $V_{LSR} = 7.4$ km s^{-1} (Table 2). One H_2O maser spot is coincident with VLA 3 ($S_\nu = 60$ mJy, $V_{LSR} = 10.7$ km s^{-1}), while the other nine spots are distributed away from the central region ($\gtrsim 4''$ [8000 AU]) and are not coincident with any known radio continuum source.

Finally, from the spatio-kinematic information of the 29 H_2O maser spots we do not observe any clear velocity segregation on scales of $\sim 13'' \times 7''$ that could indicate the presence of a systematic velocity gradient at these scales.

4. DISCUSSION

The presence of a rotating disk in the W75N(B) region was suggested by Haschick et al. (1981) from the velocity field of the OH masers, showing a north-south velocity gradient of ~ 10 km s^{-1} in $\sim 1''.5$. However, this was not confirmed in subsequent studies by Baart et al. (1986) with more sensitive data. These authors also detected an almost east-west group of OH masers, with approximately the same spatial extension as the north-south group and also without any obvious velocity gradient.

Our H_2O maser data do not support the presence of a north-south rotating disk at these scales around W75N(B). There is no north-south velocity gradient. Furthermore, the H_2O masers are distributed in clusters, suggesting different exciting sources rather than a common origin.

We discuss below, separately, the three radio continuum sources and their associated maser emission (§§ 4.1, 4.2, and 4.3). We address, in addition, the question of which of these radio continuum sources is the best candidate to power the extended CO bipolar molecular outflow. We also compare (§ 5) the H_2O maser distribution with that of the OH masers found by Baart et al. (1986). This comparison leads us to suggest that the H_2O masers around YSOs could trace either disks or outflows depending on the evolutionary stage of the young stellar exciting source (§ 6).

4.1. *VLA 1[W75N(Ba)]–H_2O Maser System*

The elongated emission of VLA 1 resembles that of the radio jets found in other YSOs (e.g., Cepheus A HW2; Rodríguez et al. 1994; Torrelles et al. 1996). The spectral index we estimate for this source from 3.6 to 1.3 cm wavelength is $\alpha_{(3.6-1.3\,cm)} \simeq 0.7$ (Table 1), which is consistent with that expected for an optically partially thick ionized thermal biconical jet according to the model of Reynolds (1986). In fact, this model predicts that for a jet of constant velocity, temperature, and ionization fraction, the flux density and length of the jet as a function of frequency scales as $S_\nu \propto \nu^{1.3-0.7/\epsilon}$ and $\theta_\nu \propto \nu^{-0.7/\epsilon}$, respectively, where ϵ is the power-law index describing the width of the jet (perpendicular to the major axis) as a function of the distance to its origin. For $\epsilon = 1$, that is, a conical jet with constant opening angle, $S_\nu \propto \nu^{0.6}$ is obtained, which is similar to that found in VLA 1. Furthermore, from these relations, and from the size observed at 1.3 cm (Table 1), a size of $\theta_\nu \sim 0''.8$ is expected at 3.6 cm, which is consistent with the value reported at this frequency ($0''.69 \pm 0''.11$, Hunter et al. 1994).

Note that VLA 1 is elongated (P.A. $\simeq 43°$) approximately in the direction of the bipolar molecular outflow observed at scales of $\sim 2'$ (roughly with P.A. $\simeq 66°$; Hunter et al. 1994). This result gives additional support that VLA 1 is a radio jet located at the base of the large-scale molecular outflow.

In fact, within the "unified" stellar jet/molecular outflow scenario of Raga et al. (1993), the molecular outflow would trace a turbulent envelope around the jet, with a deposition of momentum from the jet into that envelope. In this sense, we can estimate the mass-loss rate of the jet following Reynolds (1986). We assume a pure hydrogen jet with constant opening angle ($\epsilon = 1$), terminal velocity, and ionization fraction, as well as constant electron temperature, taken to be equal to 10^4 K. We further assume that the jet axis is perpendicular to the line of sight (that is, with an inclination angle of $i = 90°$), since variations in i from 45° to 90° change the mass-loss estimate by less than 10%. Given the elongated appearance of the jet, it is unlikely that i has values that are much smaller than 45°.

Under these assumptions, the mass-loss rate in the jet is given by

$$\dot{M}_{-6} = 1.9 V_3 x_0^{-1} S_{mJy}^{0.75} \nu_9^{-0.45} d_{kpc}^{1.5} \theta_0^{0.75} ,$$

where $\dot{M}_{-6}$ is the mass-loss rate in $10^{-6}\ M_\odot$ yr^{-1}, V_3 is the terminal velocity of the jet in 10^3 km s^{-1}, x_0 is the ionization fraction, S_{mJy} is the observed flux density in mJy, ν_9 is the observed frequency in GHz, d_{kpc} is the distance to the source in kpc, and θ_0 is the opening angle in radians.

The opening angle is estimated to be

$$\theta_0 = 2 \tan^{-1}(\theta_{min}/\theta_{maj}) ,$$

where θ_{min} and θ_{maj} are the deconvolved minor and major axes of the jet. For VLA 1 we obtain $\theta_0 \sim 30°$.

From the parameters obtained for VLA 1 (Table 1), $d_{kpc} = 2$, and $x_0 = 1$, we obtain $\dot{M}_{-6} = 4V_3$. The large luminosity observed in the W75N(B) region (a few times $10^5\ L_\odot$) indicates the presence of massive OB-type stars (Moore et al. 1988). Assuming then $V_3 = 1$, similar to that found in other young massive stars (e.g., Martí et al. 1993, 1995), $\dot{M}_{-6} = 4$ is derived for the ionized wind of VLA 1. The momentum rate that this ionized wind would deposit into the ambient medium is $\dot{P} \simeq 4 \times 10^{-3}\ M_\odot$ yr^{-1} km s^{-1}. This value is a factor of ~ 5 smaller that the momentum rate in the large-scale bipolar molecular outflow (Hunter et al. 1994). However, considering that jets (if they are shock ionized) may be only partially ionized at a level of 10%–20% ($x_0 = 0.1$–0.2; Rodríguez et al. 1990), we favor the conclusion that the VLA 1 jet is driving the large-scale bipolar molecular outflow, supporting the jet/molecular outflow models of Chernin & Masson (1991) and Raga et al. (1993).

The nature of a radio jet for VLA 1 is also supported by the spatial distribution of the H_2O masers in the cluster around this source. In Figure 4 we show the contour map of the VLA 1 source, where dots indicate the positions of the nearby H_2O masers. From this figure we see that these masers are distributed along the direction of the major axis of VLA 1. The maximum separation of this chain of 11 maser spots with respect to the major axis of VLA 1 is $\lesssim 0''.2$ ($\lesssim 400$ AU), while the mean separation is $0''.05$ (100 AU). The alignment between the radio continuum emission and the H_2O masers suggests that the latter are being excited by the wind of VLA 1 and are consequently delineating the

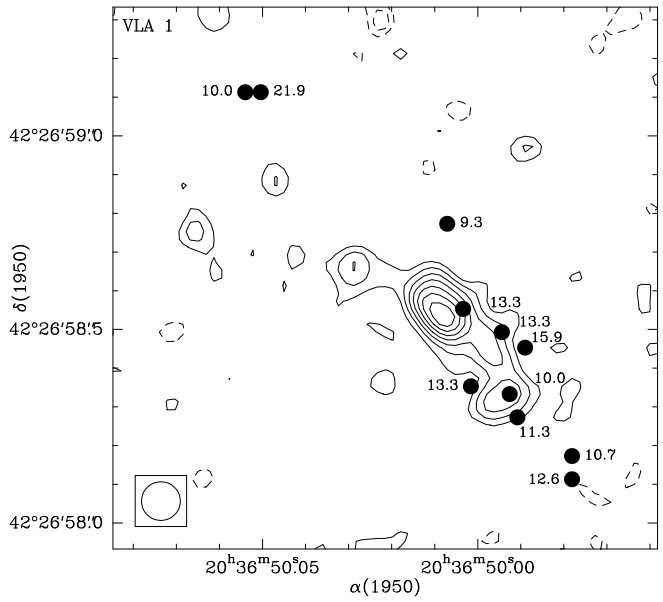

FIG. 4.—1.3 cm continuum contour map of the VLA 1 thermal radio jet. Contours are −3, −2, 2, 3, 4, 5, 6, 7, 8 times 0.16 mJy beam^{-1}, the rms of the map (beam = 0".1, shown in the lower left-hand corner). Dots indicate the position of the 11 H_2O masers detected in this particular area. The velocities of the masers are also indicated.

outflow at scales of ∼1" (2000 AU). In this scenario the H_2O masers would be pumped by the kinetic energy of the wind of VLA 1 released into the shocked circumstellar gas (see, e.g., Elitzur 1995 for this kind of H_2O maser pumping mechanism). This scenario has also been proposed to explain the H_2O maser distribution in W49N and L1448C (Gwinn 1994; Chernin 1995).

A possible objection to the common origin for the VLA 1 radio source and the nearby H_2O masers (both driven by the same wind) would be the absence of a velocity gradient in the masers along the axis of the jet. However, this can be explained if the maser spots represent dense material shocked by the wind but not significantly accelerated because of its relatively large mass and/or its being embedded in some larger clump. This possibility could be supported by the fact that the mean velocity of these H_2O masers is 12.9 km s^{-1}, close to the ambient cloud velocity traced in CS (V_{LSR} = 10 km s^{-1}; Hunter et al. 1994). In addition, the velocity dispersion we find for the H_2O masers is relatively small, 3.4 km s^{-1}. This velocity dispersion might be provided by turbulent motions of the ambient gas around VLA 1. A similar interpretation has been given for W49N, where Gwinn (1994) distinguishes between high- and low-velocity masers, with the high-velocity features arising in less dense material and more strongly accelerated by the wind than the low-velocity features, arising in more dense ambient material.

An absence of velocity gradients in the H_2O masers along the line of sight could also be explained if the outflow at these scales (∼1") has an inclination angle $i \simeq 90°$, that is, in the plane of the sky. A possible scenario is that the H_2O masers reside in a cylindrical shell around the jet. Limb-brightening effects, with a velocity-coherent gain path for the masers, would then favor the observation of masers at the edges of the shell with respect to the line of sight. In that case, radial expansion of the shell would mean that the motions of the masers would be predominantly across the line of sight. Hence, masers associated with the expansion of the jets across the jet axis would have low radial motions. Of course, even in the absence of such geometrical arguments, the fact that the jets appear to be confined radially implies that radial motions will be small. At positions far away (∼2') from VLA 1, larger radial velocities are observed, for example, within the large-scale molecular outflow. This is likely due to a widening of the jet opening angle at larger distances as well as to the sweeping of gas at the working surfaces of the jets.

4.2. *VLA 2–H_2O Maser System*

This compact continuum source of $\lesssim$0".1 size has a spectral index $\alpha_{(3.6-1.3\,cm)} \gtrsim 1$ (Table 1), which is consistent with VLA 2 being an ultracompact optically thick H II region. Some of the physical parameters of this radio source can be computed from their flux density values at 3.6 (upper limit) and 1.3 cm, assuming that it is homogeneous, isothermal ($T = 10^4$ K), and with spherical symmetry. In this way we estimate opacities of $\tau_{1.3\,cm} \gtrsim 0.6$ and $\tau_{3.6\,cm} \gtrsim 5$, and a size for the source of 0".03 (consistent with the upper limit value of our observations, $\lesssim$0".1). In addition, we also derive an electron density of $N_e \simeq 2 \times 10^6$ cm^{-3}, ionized mass of $M_{H\,II} \simeq 1 \times 10^{-5}\ M_\odot$, as well as the rate of ionizing photons required to maintain this region fully ionized, $N_i \simeq 7 \times 10^{45}$ s^{-1}. These ionizing photons can be provided by a zero-age main-sequence (ZAMS) B0.5 or earlier star (Panagia 1973).

Indirect evidence for the presence of a wind in this source comes from the association of the cluster of eight H_2O maser spots with VLA 2, if these masers are shock excited by a wind. These masers are distributed in a shell of ∼0".18 × 0".10 (R.A. × decl.; 360 × 200 AU) around the continuum source (see Fig. 5), which is a more compact distribution than that observed in VLA 1 (§ 4.1). For these masers we estimate a mean velocity of V_{LSR} = 7.1 km s^{-1} and a velocity dispersion of 5.9 km s^{-1}. This velocity dispersion can be bound by a mass of 8 $M_\odot$ in a radius of 200 AU around VLA 2, which can be provided by a central B0.5 or earlier star and/or the associated circumstellar gas.

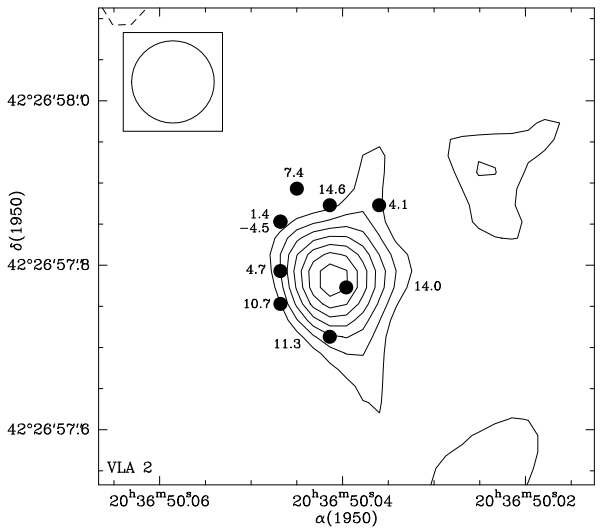

FIG. 5.—1.3 cm continuum contour map of VLA 2. Contours are −3, −2, 2, 3, 4, 5, 6, 7, 8 times 0.16 mJy beam^{-1}, the rms of the map (beam = 0".1, shown in the top left-hand corner). Dots indicate the position of the eight H_2O maser spots detected in this particular area. The velocities of the masers are also indicated.

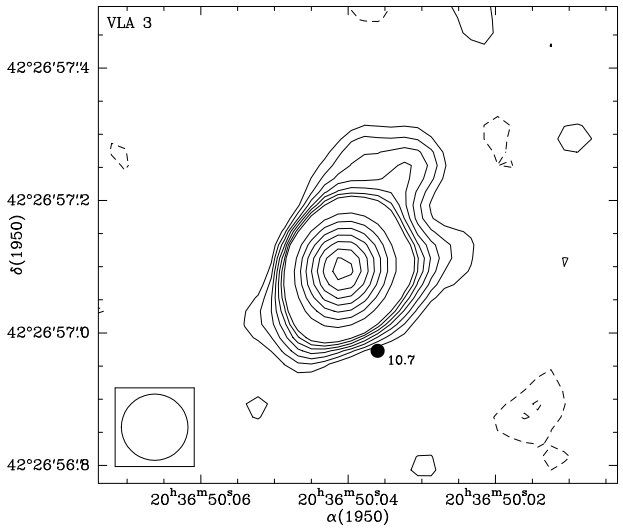

FIG. 6.—1.3 cm continuum contour map of VLA 3. Contours are −3, −2, 2, 3, 4, 5, 6, 7, 8, 15, 20, 25, 30, 35, 40, 45 times 0.16 mJy beam^{-1}, the rms of the map (beam = 0".1, shown in the top right-hand corner). The dot indicates the position of the H_2O maser spot detected in this particular area. The velocity of the maser is also indicated.

Interestingly, there is a rough north-south velocity segregation in the H_2O masers, with the northern spots blue-shifted by ~ 8 km s^{-1} with respect to the southern ones (see Fig. 5), that is, along the major axis of the shell. This segregation in velocity could indicate systematic motions in the masers. Unfortunately, however, we do not have additional information to distinguish if they are tracing rotating, contracting, or even expanding motions. In the case of bound motions, the maser spots could be located in a rotating and/or contracting high-density circumstellar structure of 200 AU radius (e.g., a circumstellar disk), pumped by the shocks of a central wind, and tracing the kinematics of the circumstellar gas (as suggested in Cepheus A HW 2, Torrelles et al. 1996). It therefore seems clear that higher angular resolution observations are needed to resolve the morphology of the continuum emission of VLA 2. If so, it may be possible to discern any preferential direction of the radio emission in VLA 2 (radio jet?) and its relation to the H_2O maser system.

4.3. *VLA 3[W75N(Bb)]–H_2O Maser System*

Both the deconvolved size, 0".09 × 0".04 (P.A. 152°), and the spectral index derived, $\alpha_{(3.6-1.3\,\mathrm{cm})} = 1.6$ for this continuum source (Table 1), suggest that it is an ultracompact optically thick H II region. Under the same assumptions as those made for VLA 2 (see § 4.2), we derive for VLA 3 a size of 0".08 (consistent with the observed deconvolved size), opacities of $\tau_{1.3\,\mathrm{cm}} \gtrsim 1$, $\tau_{3.6\,\mathrm{cm}} \gtrsim 11$, electron density of $N_e \simeq 2 \times 10^6$ cm^{-3}, ionized mass of $M_{\mathrm{HII}} \simeq 1 \times 10^{-4}\ M_\odot$, and rate of ionizing photons of $N_i \simeq 6 \times 10^{46}$ s^{-1} (which can be provided by a ZAMS B0 or earlier star).

A relatively weak water maser spot of 60 mJy with $V_{\mathrm{LSR}} = 10.7$ km s^{-1} is observed $\sim 0".13$ south from VLA 3 (Fig. 6). Given the characteristics of the radio continuum emission of this source and its relatively low activity in H_2O masers, we cannot infer for it the presence of a wind.

5. H_2O MASER–OH MASER DISTRIBUTION

Another important issue that can be addressed with the present data is the relationship between H_2O and OH masers in W75N(B). Measuring the relative positions of the OH and H_2O masers with respect to the position of the YSOs in star-forming regions is a crucial key for understanding their formation and excitation (see Forster & Caswell 1989). Baart et al. (1986), by comparing the distribution of the OH masers with respect to the 6 cm continuum emission of W75N(B) (beam = 1".5, Haschick et al. 1981), proposed that these masers could trace the edges of an expanding H II region. However, because of the relatively low angular resolution of their radio continuum observations, Baart et al. (1986) noted, as an important future goal, that new higher angular resolution observations could clarify the structure of the ionized gas and its relationship with the OH masers. With our high angular resolution and high-sensitivity observations, we are able now to carry out that suggested study.

In Figure 7 we plot the positions of the OH masers found by Baart et al. (1986) together with the positions of the H_2O maser and 1.3 cm continuum sources detected in the same region. From the absolute positional errors quoted by Baart et al. (1986) for the OH masers, we estimate that the error in the relative alignment between the OH and the H_2O positions should not exceed 0".1. This error does not affect any of the conclusions discussed below.

From Figure 7 we see that the OH masers are also distributed in groups near the 1.3 cm continuum sources. In general, the OH masers are close to the H_2O masers, but they are not spatially coincident. Analyzing individually each region near the radio continuum sources, if we trace a line from VLA 1 with the same orientation as the major axis of the radio jet (see Fig. 7), we identify a chain of groups of OH masers located on both sides of this line. We note that the H_2O masers appear located closer to the axis defined by the outflow of VLA 1 than the OH masers. In fact, the angular distance of the H_2O masers to this axis is $\lesssim 0".2$,

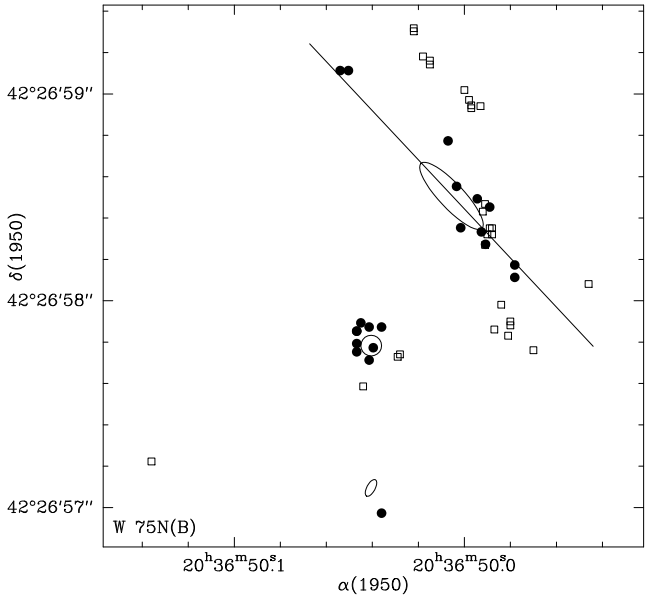

FIG. 7.—Map showing the position of the H_2O masers (*dots*) in the region where OH masers (*squares*) where detected (Baart et al. 1986). The size and elongation of the VLA 1 thermal radio jet is represented by an ellipse. The line indicates the direction of the outflow, drawn to assist the discussion in § 4. The positions of VLA 2 and VLA 3 are indicated by a circle and a small ellipse, respectively. Other nine H_2O masers detected at distances $\gtrsim 4''$ from the continuum sources do not appear in this figure.

while the OH masers are located at distances of $\lesssim 0''.4$. We think that this H_2O-OH maser distribution with respect to the VLA 1 radio jet, and specifically that the two groups intersect the jet, suggests a common origin for both kinds of masers, i.e., both masers were pumped by the energy released in shocks in the ambient medium by the wind of VLA 1. We propose that both the H_2O and OH masers trace the outflow axis of the VLA 1 source, with the OH masers being excited in the outer parts of the jet. This could be consistent with the scenario proposed by Forster & Caswell (1989) in which the OH maser emission in star-forming regions would be produced later than the H_2O masers, but in a less dense circumstellar material surrounding the YSOs.

We have also considered an alternative scenario for the H_2O-OH maser distribution around VLA 1 in which the OH masers define a different axis (P.A. $\simeq 10°$), as compared with the axis defined by the H_2O masers. The OH masers could then trace an "older" outflow from a large precessing VLA 1 source. And, of course, we cannot rule out the possibility that the OH and H_2O masers are driven by different exciting sources. However, in that case, one of the exciting sources remains undetected in the radio continuum.

With respect to VLA 2, three OH maser spots are located near this source ($\lesssim 0''.2$) and their associated cluster of H_2O masers (see Fig. 7), suggesting, as in VLA 1, a common exciting source (VLA 2) for both types of masers. Again the OH masers are more separated ($\lesssim 0''.2$) with respect to VLA 2 than the H_2O masers ($\lesssim 0''.1$), consistent with the latter forming in a denser environment surrounding the YSO.

Finally, there is no OH maser spot spatially associated with VLA 3, although an OH spot is observed $\sim 1''$ east from both VLA 2 and VLA 3.

In summary, we think that most of the H_2O-OH maser distribution observed in the region and shown in Figure 7 can be explained by having three centers of activity, VLA 1, VLA 2, and VLA 3. Furthermore, we think that it is also possible that most of the nine H_2O maser spots observed at distances $\gtrsim 4''$ ($\gtrsim 8000$ AU; see Fig. 3) from the continuum sources could also be produced by the wind of VLA 1 (especially those distributed northeast-southwest), once the opening angle of the wind becomes larger farther out as the pressure of the external medium decreases.

6. GENERAL CONSIDERATIONS

It is well known that the first stages of evolution of YSOs are characterized by strong outflows in the presence of high-density circumstellar disks formed around them. Many of the phenomena and characteristics observed in star-forming regions (e.g., infall and rotating motions of the circumstellar gas around YSOs, jets, molecular outflows, Herbig-Haro objects, H_2O and OH masers) can be explained within a general scenario consisting of the formation of a disk-YSO-outflow system and its subsequent interaction with the ambient medium (e.g., Lizano & Torrelles 1995). In particular, H_2O maser emission requires physical conditions in the gas of a few times 100 K in the kinetic temperatures and densities of $n(H_2) \gtrsim 10^9$ cm^{-3} (e.g., Elitzur 1995). These physical conditions can be reached in both the inner parts of the circumstellar disks around YSOs and in the shocked gas within the associated wind. Therefore, a priori, H_2O masers in star-forming regions could trace both the outflow (e.g., as suggested in W3OH, Alcolea et al. 1992; W49N, Gwinn 1994; and L1448C, Chernin 1995) and/or the circumstellar disk surrounding the YSOs (e.g., as suggested in Orion-KL, Abraham & Vilas Boas 1994; IRAS 00338+6312, Fiebig et al. 1996; and Cepheus A HW2, Torrelles et al. 1996). Interestingly, this dichotomy seems to be present also in galaxies with water megamasers. While in NGC 4258 Miyoshi et al. (1995) find that the H_2O maser emission traces a subparsec-scale disk in Keplerian rotation around the nucleus of the galaxy, in NGC 1052 the masers are aligned along the same axis as the continuum jet that emanates from the galactic core (Braatz et al. 1996).

However, if H_2O masers can trace both the direction of the outflows and/or the circumstellar disks around YSOs, is there any physical reason to explain why in a particular region the masers "prefer" to trace selectively either the outflow or the disk? Based on the data presented in this paper, and from the evolutionary scenario proposed by Forster & Caswell (1989) to explain the spatial relationship of OH and H_2O masers found in star-forming regions, we have considered below the possibility that the H_2O masers could trace either the outflow or the circumstellar disk depending on the evolutionary stage of its associated YSO. However, it should be noted that other effects (e.g., the luminosity of the embedded sources) could play an important role to produce this dichotomy and certainly it deserves further investigation.

According to Forster & Caswell (1989), H_2O masers appear first in the high-density circumstellar material of YSOs, followed later by OH emission forming in less dense material surrounding the core. This simple H_2O-OH maser association around YSOs lasts about 10^5 yr. After that time, the H_2O and OH masers are dispersed at larger scales over the next 10^4 yr. This dispersion could be due to the action of winds of the YSOs and/or due to expanding motions of the associated H II regions. In W75N(B), three young objects traced by VLA 1, VLA 2, and VLA 3 are found. VLA 1 is related to a "rich" activity in H_2O and OH maser, with a relatively large spatial dispersion along the direction of the outflow. On the other hand, VLA 2 has also an important activity in H_2O and OH maser emission, but with a lower spatial dispersion and less intensity than in the corresponding masers of VLA 1. Finally, VLA 3 has associated only an H_2O maser, without any known OH maser. Taking all this in mind, we tentatively propose an evolutionary sequence for these objects. VLA 3 would be the "youngest" source of the W75N(B) star-forming region, not having had time to develop H_2O and OH maser activity. VLA 1, at the other extreme, would be the "oldest" source of this region, with its associated H_2O and OH masers already tracing the outflow. This would also be consistent with VLA 3 being an ultracompact optically partially thick and less developed H II region, with VLA 1 being an optically partially thick, more developed ionized wind at the base of the large-scale molecular outflow (§§ 4.1 and 4.3). For this molecular outflow, a dynamical time of $\sim 10^4$ yr has been derived (Hunter et al. 1994). Between these two objects, following this evolutionary sequence, would be VLA 2, with its associated masers probably tracing bound motions in the surrounding circumstellar gas (a rotating/contracting disk? § 4.2).

If this evolutionary sequence applies, it would imply that objects like Cepheus A HW 2 and IRAS 00338+6312, with their H_2O masers tracing circumstellar disks, would be relatively less evolved that those objects where the masers already trace the motions of the outflows (e.g., W49N, W3OH, L1448C).

It seems therefore clear that the identification of further star-forming regions, with the presence of multiple YSOs and H_2O and OH maser emission, in order to make similar studies to those presented in this paper, would certainly help to clarify the evolutionary scenario suggested by the present work.

7. CONCLUSIONS

We report VLA-A 1.3 cm continuum and H_2O maser observations toward W75N(B) with 0".01 resolution. The strongest H_2O maser component of the source was used to self-calibrate its signal, and we then applied their phase and amplitude corrections to the 1.3 cm continuum data (cross-calibration). With this technique we improved the signal-to-noise ratio of the continuum data by a factor of 1.6, detecting three radio continuum sources in a region of $\sim$1".5, namely, VLA 1, VLA 2, and VLA 3. In addition, 29 H_2O maser spots are detected in the region, most of them distributed in two clusters associated with VLA 1 and VLA 2. We have also compared the H_2O and OH (detected previously in the region) maser distributions. Our main conclusions can be summarized as follows:

The characteristics of VLA 1 are consistent with a thermal biconical jet, oriented in the direction of the large-scale ($\sim$2') bipolar molecular outflow. The distribution of the H_2O masers associated with this source, along the major axis of the jet, suggests that they are tracing the outflow at scales of $\sim$1". We propose that VLA 1 is the powering source of the molecular outflow.

The H_2O masers associated with VLA 2 (unresolved continuum source) are distributed in a compact "shell" of $\sim$0".2 size. Their observed velocities could represent bound motions around VLA 2. An H_2O maser spot is detected toward VLA 3.

Both circumstellar disks and outflows have been inferred in the literature from the distribution of H_2O masers around YSOs. We have considered the possibility that the dichotomy in the relation between H_2O masers and jets could be the result of evolutionary effects, with masers in less evolved objects tracing bound motions and more evolved ones tracing outflows. The identification of further star-forming regions, with the presence of multiple YSOs and H_2O and OH maser emission, followed by similar studies to those presented in this paper would certainly help to clarify this important issue.

We would like to thank Mark Claussen for many useful and valuable comments. S. C. acknowledges the support of CONACyT grant 400354-5-1023-PE and DGAPA grant IN101695. J. F. G., J. M. T., and R. V. are supported in part by DGICYT grant PB 95-0066 and by Junta de Andalucía (Spain). P. T. P. H. is supported in part by NASA grant NAGW-3121. L. F. R. acknowledges the support of DGAPA, UNAM, and CONACyT, México. R. V. thanks Agencia Española de Cooperación Internacional for his graduate scholarship and DGAPA-UNAM for complementary support.

REFERENCES

Abraham, Z., & Vilas Boas, J. W. S. 1994, A&A, 290, 956
Alcolea, J., Menten, K. M., Moran, J. M., & Reid, M. J. 1992, in Astrophysical Masers, ed. A. W. Clegg & G. E. Nedoluha (Heidelberg: Springer), 225
Anglada, G. 1995, in Rev. Mexicana Astron. Astrophys. Ser. Conf. 1, Circumstellar Disks, Outflows and Star Formation, ed. S. Lizano & J. M. Torrelles (México: Instituto de Astronomía, UNAM), 67
———. 1996, in ASP Conf. Ser. 93, Radio Emission from the Stars and the Sun, ed. A. R. Taylor & J. M. Paredes (San Francisco: ASP), 3
Baart, E. E., Cohen, R. J., Davies, R. D., Norris, R. P., & Rowland, P. R. 1986, MNRAS, 219, 145
Braatz, J., Claussen, M., Diamond, P., Wilson, A., & Henkel, C. 1996, BAAS, 189, 8906
Chernin, L. M. 1995, ApJ, 440, L97
Chernin, L. M., & Masson, C. R. 1991, ApJ, 382, L39
Curiel, S., Rodríguez, L. F., Cantó, J., Bohigas, J., Roth, M., & Torrelles, J. M. 1989, Astrophys. Lett. Commun., 27, 299
Curiel, S., Rodríguez, L. F., Moran, J. M., & Cantó, J. 1993, ApJ, 415, 191
Elitzur, M. 1995, in Circumstellar Disks, Outflows and Star Formation, ed. S. Lizano & J. M. Torrelles (México: Instituto de Astronomía, UNAM), 85
Forster, J. R., & Caswell, J. L. 1989, A&A, 213, 339
Fiebig, D., Duschl, W. J., Menten, K. M., & Tscharnuter, W. M. 1996, A&A, 310, 199
Gómez, J. F., Curiel, S., Torrelles, J. M., Rodríguez, L. F., Anglada, G., & Girart, J. M. 1994, ApJ, 436, 749
Gwinn, C. R. 1994, ApJ, 429, 241
Harvey, P. M., Campbell, M. F., & Hoffman, W. F. 1977, ApJ, 211, 786
Habing, H. J., Goss, W. M., Matthews, H. E., & Winnberg, A. 1974, A&A, 35, 1
Haschick, A. D., Reid, M. J., Burke, B. F., Moran, J. M., & Miller, G. 1981, ApJ, 244, 76
Hunter, T. R., Taylor, G. B., Felli, M., & Tofani, G. 1994, A&A, 284, 215
Johnston, K. J., Sloanaker, R. M., & Bologna, J. M. 1973, ApJ, 182, 67
Lizano, S., & Torrelles, J. M. 1995, Rev. Mexicana Astron. Astrophys. Ser. Conf. 1, Circumstellar Disks, Outflows and Star Formation (México: Instituto de Astronomía, UNAM)
Lekht, E. E. 1995, Astronomy Reports, 39, No.1, 27
Martí, J., Rodríguez, L. F., & Reipurth, B. 1993, ApJ, 416, 208
———. 1995, ApJ, 449, 184
Miyoshi, M., Moran, J. M., Herrnstein, J., Greenhill, L., Nakai, N., Diamond, P., & Inoue, M. 1995, Nature, 373, 127
Moore, T. J. T., Mountain, C. M., Yamashita, T., & Selby, M. J. 1988, MNRAS, 234, 95
Panagia, N. 1973, AJ, 78, 929
Pravdo, S. H., Rodríguez, L. F., Curiel, S., Cantó, J., Torrelles, J. M., Becker, R. H., & Sellgren, K. 1985, ApJ, 293, L35
Raga, A. C., Cantó, J., Calvet, N., Rodríguez, L. F., & Torrelles, J. M. 1993, A&A, 276, 539
Reid, M. J., & Menten, K. M. 1990, ApJ, 360, L51
Reynolds, S. P. 1986, ApJ, 304, 713
Rodríguez, L. F., Garay, G., Curiel, S., Ramírez, S., Torrelles, J. M., Gómez, Y., & Velázquez, A. 1994, ApJ, 430, L65
Rodríguez, L. F., Ho, P. T. P., Torrelles, J. M., Curiel, S., & Cantó, J. 1990, ApJ, 352, 645
Thompson, A. R., Moran, J. M., & Swenson, G. W. 1986, in Interferometry and Synthesis in Radio Astronomy (New York: John Wiley & Sons), 240
Tofani, G., Felli, M., Taylor, G. B., & Hunter, T. R. 1995, A&AS, 112, 299
Torrelles, J. M., Gómez, J. F., Rodríguez, L. F., Curiel, S., Ho, P. T. P., & Garay, G. 1996, ApJ, 457, L107
Torrelles, J. M., Ho, P. T. P., Rodríguez, L. F., & Cantó, J. 1985, ApJ, 288, 595
Wynn-Williams, C. G., Becklin, E. E., & Neugebauer, G. 1974, ApJ, 187, 473